EXPERIMENTAL TECHNIQUE AND DEVICES

Original article
DOI: https://doi.org/10.18721/JPM.18304

A DETECTOR OF MICROMETEOROIDS AND SPACE DEBRIS PARTICLES BASED ON A FILM INDUCTANCE COIL

A. M. Telegin✉, *M. P. Kalaev*

Samara National Research University, Samara, Russia

✉ talex85@mail.ru

Abstract. In the paper, a model of a detector of high-speed microparticles (micrometeoroids and space debris) is proposed, made in the form of a round spiral film inductance coil. The design of the gauge ensures the creation of frequency resonance that occurs when the metal strip of the coil is broken. The obtained results of a laboratory and computer simulations of the detector showed that the film coil is suitable for recording high-speed microparticles larger than 100 μm on a spacecraft such as CubeSat. The fracture point of the inductance coil can be found by analyzing the shift of the resonant frequency of the amplitude-frequency characteristic. In this case, the reliable determination of the point becomes possible if the number of the broken turn is greater than 5.

Keywords: micrometeoroid, space debris, inductance coil, crater, spacecraft, laboratory simulation

Citation: Telegin A. M., Kalaev M. P., A detector of micrometeoroids and space debris particles based on a film inductance coil, St. Petersburg State Polytechnical University Journal. Physics and Mathematics. 18 (3) (2025) 49–59. DOI: https://doi.org/10.18721/JPM.18304

Научная статья
УДК 621.384.62
DOI: https://doi.org/10.18721/JPM.18304

ДАТЧИК МИКРОМЕТЕОРОИДОВ И ЧАСТИЦ КОСМИЧЕСКОГО МУСОРА НА ОСНОВЕ ПЛЕНОЧНОЙ КАТУШКИ ИНДУКТИВНОСТИ

А. М. Телегин✉, *М. П. Калаев*

Самарский национальный исследовательский университет имени академика С. П. Королёва, г. Самара, Россия

✉ talex85@mail.ru

Аннотация. В работе предложена модель датчика высокоскоростных микрочастиц (микрометеороидов и частиц космического мусора) в виде круглой спиральной пленочной катушки индуктивности. Конструкция датчика обеспечивает создание частотного резонанса, возникающего при разрыве металлической полоски катушки. Полученные результаты компьютерного и лабораторного моделирования данной конструкции показали, что пленочная катушка пригодна для регистрации высокоскоростных микрочастиц размерами более 100 мкм на космических аппаратах типа CubeSat. Место разрыва металлической полоски катушки индуктивности можно определять с помощью анализа сдвига резонансной частоты амплитудно-частотной характеристики. При этом надежное определение места разрыва становится возможным, если номер разорванного витка больше 5.

Ключевые слова: микрометеороид, космический мусор, катушка индуктивности, кратер, космический аппарат, лабораторное моделирование

Ссылка для цитирования: Телегин А. М., Калаев М. П. Датчик микрометеороидов и частиц космического мусора на основе пленочной катушки индуктивности // Научно-технические ведомости СПбГПУ. Физико-математические науки. 2025. Т. 18. № 3. С. 49—59. DOI: https://doi.org/10.18721/JPM.18304

Introduction

Spacecraft engineering must anticipate how various factors in the space environment influence the structural components and onboard electronics. To address this, ground-based laboratories are established, space experiments are conducted, and models of the behavior of materials in outer space are constructed. Besides various types of space radiation (protons, electrons, etc.), spacecraft are also bombarded by space debris and micrometeoroids. Typically, multilayer structures with specialized coatings (such as thermal control coatings, heat pipes, heat exchangers, optical glasses, solar panels, antennas, electric vacuum insulation, etc.) make up the elements of spacecraft directly exposed to these impacts. Even collisions with particles that do not penetrate these elements lead to degradation of their surfaces, gradually altering optical, electrical, and mechanical characteristics, ultimately compromising the spacecraft's performance. As lifespans of spacecraft are extended, detection of micrometeoroids and the ever-increasing amounts of man-debris, along with protection of spacecraft protection pose crucial challenges. Furthermore, the concentrations of high-speed man-made dust particles in near-Earth orbit have been growing in recent years [1—12].

Sensors based on different physical principles are used to control the distribution of microparticles (micrometeoroids and space debris particles) in near-Earth space [11—15]. Film-based detectors are of particular interest, allowing for large sensitive surface and relatively low mass [13—21].

In this paper, we consider the concept of a film detector for high-speed microparticles based on a spiral film inductor allowing to determine the impact sites of high-speed microparticles using spectral analysis of the data obtained. Only one measurement channel was used instead of a large number of multiplexers, as is customary in available equivalents [18].

Model of primary transducer (excluding parasitic parameters)

A film inductor made of conductive material deposited on a dielectric substrate is proposed as the primary transducer of the detector for high-speed microparticles (Fig. 1,*a*). The surface of the other side of the substrate is modified by metallization.

The inductance of such a circular spiral film inductor can be calculated by the following formula [22—28]:

$$L = 0.033937 \cdot \frac{a^2 \cdot n^2}{8 \cdot a + 11 \cdot c} \cdot K_g,$$

$$a = \frac{D_o + D_i}{4},\ c = \frac{D_o - D_i}{2},$$

$$K_g = 0.570 - 0.145 \cdot \ln(W/h),$$

where L, nH, is the inductance of the inductor coil; n is the number of turns in the coil; D_i, D_o, μm, are its inner and outer diameters, respectively; h, μm, is the thickness of the dielectric substrate; W, μm, is the width of the strip; (some geometric parameters are shown in Fig. 1,*a*); K_g is a factor accounting for the presence of a ground plane.

The factor K_g decreases as it approaches the ground plane, so it was assumed to be equal to unity in [24].

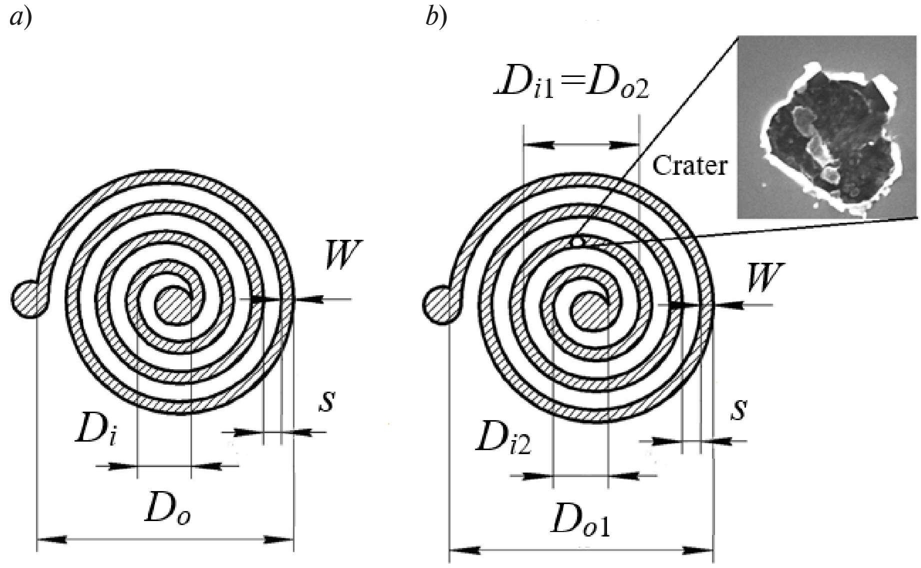

Fig. 1. Cross-sections of inductor coils without break (*a*) and with break (*b*); their geometric parameters are shown
Inset: micrograph of bowl-shaped depression (crater)

When a high-speed microparticle collides with the metal strip, a crater forms, producing a break (Fig. 1,*b*). The size of the formed crater can be roughly estimated by the empirical models presented in [29]:

$$D/d = K_1 \cdot \rho_p^{0.333} \cdot V^{0.667},$$

where K_1 is a coefficient whose value depends on the nature of the materials of the metal strip and the microparticles; D, d, cm, are the diameters of the crater and microparticles, respectively; ρ_p, g/cm^3, is the density of the incident microparticle; V, km/s, is the speed of the microparticle.

The break in the metal strip leads to the formation of an electrical capacitance series-connected to the metal strip (see Figs. 1 and 2). The nominal value of this capacitance can be calculated using model of a coplanar capacitor based on a microstrip line [30–33]:

$$C_g = \frac{1}{2} C_{even},$$

$$C_{even} = W \cdot \left(\frac{S}{W}\right)^{m_e} \cdot e^{K_e} \cdot \left(\frac{\varepsilon}{9.6}\right)^{0.9}$$

$$m_e = \frac{1.565}{(W/h)^{0.16}} - 1, \text{ for } 0.3 \le \frac{S}{W} \le 1,$$

$$K_e = 1.97 - \frac{0.03}{W/h}, \text{ for } 0.3 \le \frac{S}{W} \le 1.$$

where C_g, pF, is the capacitance of the broken strip; m_e, K_e, C_{even} are intermediate variables used for calculating the capacitance of the broken strip; S_g, μm, is the width of the break in the metal strip equal to the diameter of the crater from a high-speed collision; W, cm, is the width of the metal strip; h, mm, is the height of the dielectric substrate; ε is the dielectric constant of the material to which the strip is attached.

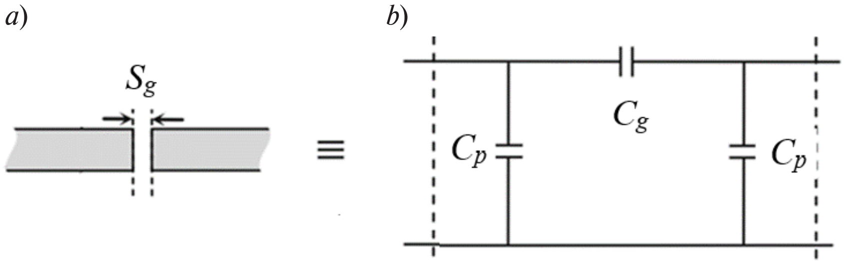

Fig. 2. Schematic model of coplanar capacitor formed from break of the metal strip (see Fig. 1) (*a*) and its equivalent circuit (*b*): S_g is the width of the strip; C_g is the capacitance of the broken strip; C_p is the parasitic capacitance of the strip relative to metallization on the other side of the dielectric substrate

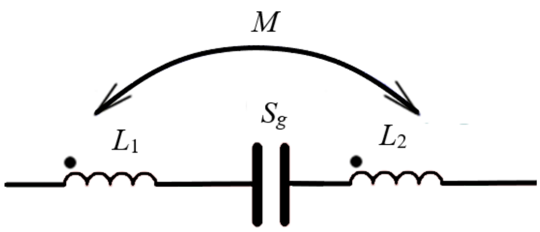

Fig. 3. Equivalent circuit of broken inductor coil: inductances of the larger and smaller coils L_1, L_2; their mutual inductance M; capacitance C_g (see Fig. 2). Each bold dot indicates the point where current flows into the inductor

Our preliminary calculations show that the capacitance of the coplanar capacitor is small compared with the turn-to-turn capacitance of the film inductor, therefore, C_g can be approximately estimated as the capacitance between two adjacent turns of the coil where break occurred (in accordance with the expressions given in [21, 34]).

Thus, a coil with a break (see Figs. 1, 2) can be represented as two inductively coupled coils, series-connected through an electrical capacitance (Fig. 3). The mutual inductance M can be estimated by the following analytical expression [25]:

$$M = \frac{\mu_0}{4\pi} N_1 \cdot N_2 \frac{D_{o1}}{(1-\theta)\cdot(\Delta-\delta)} \times$$
$$\times\left[\frac{A_3}{3}\left(\Delta^3-\delta^3\right)\cdot\ln\left(\frac{1}{\theta}\right)+\frac{A_5}{10}\left(\Delta^5-\delta^5\right)\cdot\left(\frac{1}{\theta^2}-1\right)+\frac{A_7}{28}\left(\Delta^7-\delta^7\right)\cdot\left(\frac{1}{\theta^4}-1\right)\right],$$

where N_1, N_2 are the numbers of turns in the larger and smaller coils; D_{o1}, D_{i1}, cm,are the outer and inner diameters of the larger coil, respectively; d_{o1}, d_{i1}, cm, are the outer and inner diameters of the smaller coil, respectively (see Fig. 1,*b*); $\theta = D_{o2}/D_{o1}$; $\Delta = D_{i1}/D_{o1}$; $\delta = D_{i2}/D_{o1}$; $A_3 = 9.870$, $A_5 = 3.701$, $A_7 = 2.313$ are the coefficients taken from [25].

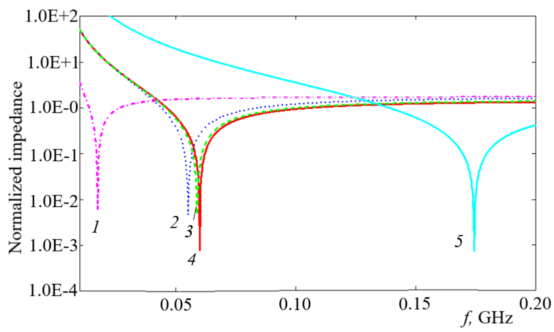

Fig. 4. Variation in normalized impedance of broken inductor coil for different pairs of parameters (ratio $k = N/N_{max}$ and capacitance C_g, pF): 0.7, 0.005 (curve *1*); 0.7, 0.05 (*2*); 0.5, 0.05 (*3*); 0.9, 0.05 (*4*); 0.7, 0.005 (*5*)

The results of computer simulation carried out using the above analytical expressions are shown in Fig. 4. It was taken into account in the simulation that the outer diameter of the coil was taken equal to 10 cm (the dimensions were chosen so that the coil could be placed on the outer wall of a CubeSat spacecraft), the inner diameter of the spiral was 1 cm, the strip width was 250 μm and the number of turns was 90. The inductance of the coil was approximately $9.65\cdot10^{-5}$ H.

The simulation results showed that the total impedance of the broken coil at high frequencies tends to the impedance of an intact coil. The resonance frequencies are clearly detected in this case. They depend on the parameters of the inductor, the location of the break and the nominal value of the resulting capacitance.

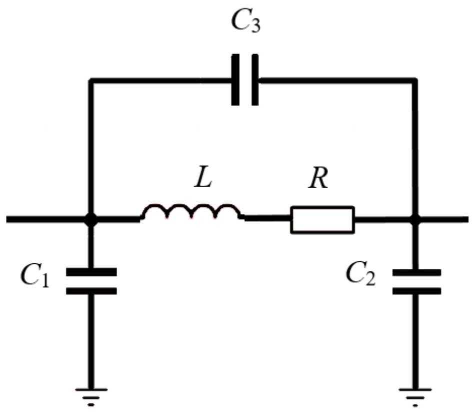

Fig. 5. Equivalent circuit of broken coil taking into account parasitic parameters: parasitic turn-to-turn capacitance C_3, parasitic coil resistance R

Model of primary transducer taking into account parasitic parameters

Each real coil has parasitic parameters: electrical capacitance and resistance, which can be estimated by the following expressions [22, 23] (Fig. 5):

$$R = \frac{K \cdot \pi \cdot a \cdot n \cdot R_{sh}}{W},$$

$$K = 1 + 0.333 \cdot \left(1 + \frac{S}{W}\right),$$

$$C_3 = 3.5 \cdot 10^{-5} \cdot D_0 + 0.06,$$

where R_{sh}, Ω/□, is the sheet resistance of the film; C_3, pF, is the parasitic turn-to-turn capacitance; S, μm, is the gap between the turns of the inductor coil; K is the correction factor accounting for current crowding in the corners of the conductor.

The simulation results for the dependence of the coil impedance on frequency (taking into account parasitic parameters) in Fig. 6 indicate that an additional resonance appears on the frequency response curve due to parasitic elements.

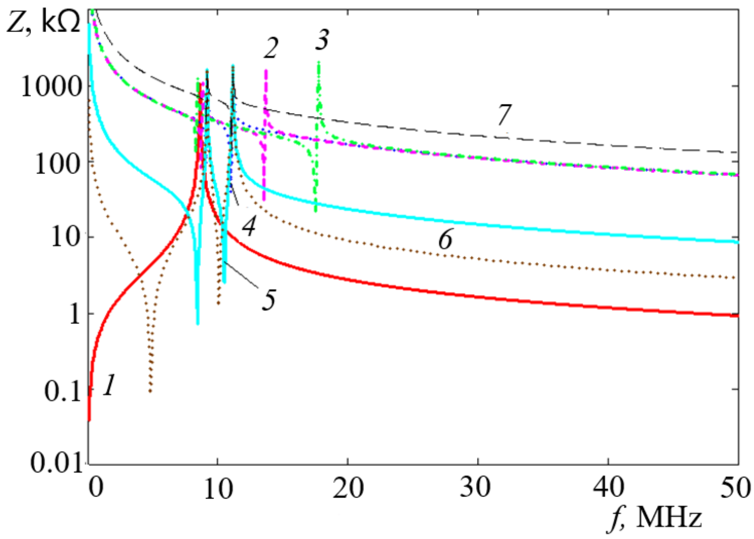

Fig. 6. Dependence of impedance on frequency (taking into account parasitic parameters) for different pairs of parameters (ratio k and capacitance C_g, pF): 0.9, 0.05 (curve *2*); 0.5, 0.05 (*3*); 0.7, 0.05 (*4*); 0.7, 0.5 (*5*); 0.7, 5.0 (*6*); 0.7, 0.025 (*7*); curve *1* corresponds to inductance without break

Experimental results

A prototype of a circular inductor coil with a diameter of 100 mm was made for the experiments (Fig. 7); a close-up photograph of the break made by a scalpel cut is also shown. The width of the metal strip was about 200 μm, the width between the strips was about 250 μm. A LiteVNA64 vector network analyzer with a frequency range of 50 kHz–6.3 GHz was used to determine the amplitude and phase characteristics of the film detector. The analyzer, bundled with the NanoVNA-App software, was connected to a personal computer. The measurement results were saved to a database on the PC and then analyzed using the GNU Octave program.

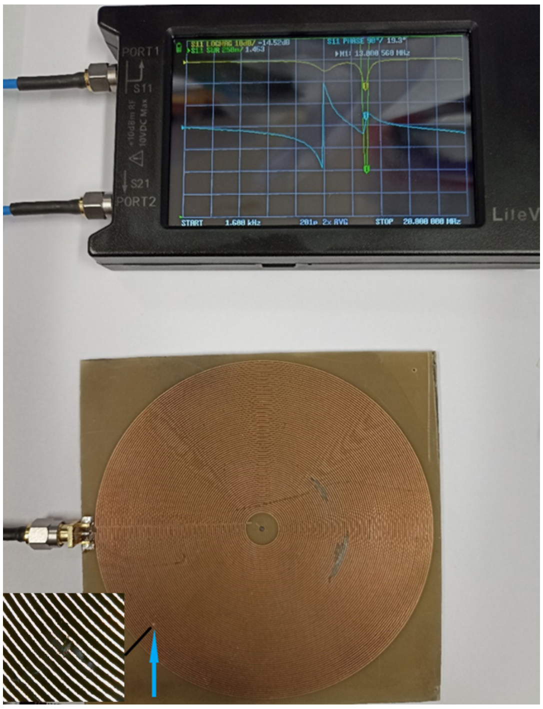

Fig. 7. Photographs of experimental waveform (top) and prototype detector (bottom) based on the inductor (the break point is marked by an arrow)

The screen shows curves of the magnitude of the total impedance, impedance phase and standing wave ratio (yellow, blue, and green lines, respectively). *Inset:* enlarged region of the coil with the break

The obtained frequency response of the film inductor for different strip parameters is shown in Fig. 8. The turn numbering starts from the outer diameter of the coil. Importantly, multiple resonances are observed. Further analysis was performed only for the first two resonances.

Fig. 9 shows the experimental dependences of the position of the first (Res1) and second (Res2) resonance peaks on the position of the break point as well as the approximation of experimental data by power functions. It can be seen that the behavior of the experimental curves obtained is in good agreement with the results of computer simulation.

As it turned out, the dependence of the resonant frequency f of the detector on the positions of the break points are well approximated by a function of the form

$$f = k/N^{\alpha},$$

where N is the turn number (numbering starts from the outer diameter of the coil); k is a constant (k_1 = 59.89, k_2= 121.34 for the first and second resonances, respectively); α is the exponent (α_1 = 0.589, α_2 = 0.571 for the first and second resonances, respectively). For small N (5–15), the resonant frequency shift reaches 1 MHz per turn, so that not only the radial position of the particle impact area, but also its sector (part of the arc length when the number N is not an integer) is determined with high accuracy. For large N (60–75), the resonant frequency shift is on the order of 20 kHz per turn, also allowing to determine the particle's impact sector, albeit with a lower accuracy.

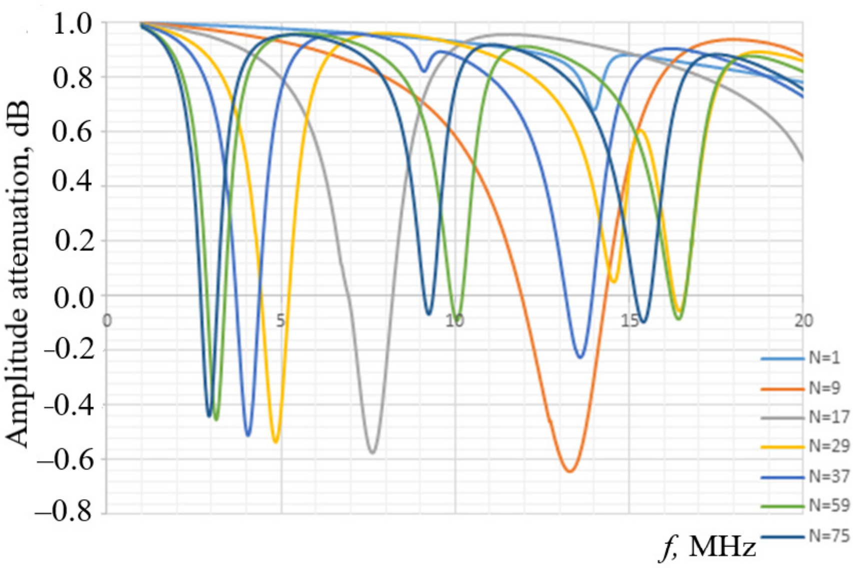

Fig. 8. Frequency response of film inductor with different broken turns (N is the number of the broken turn)

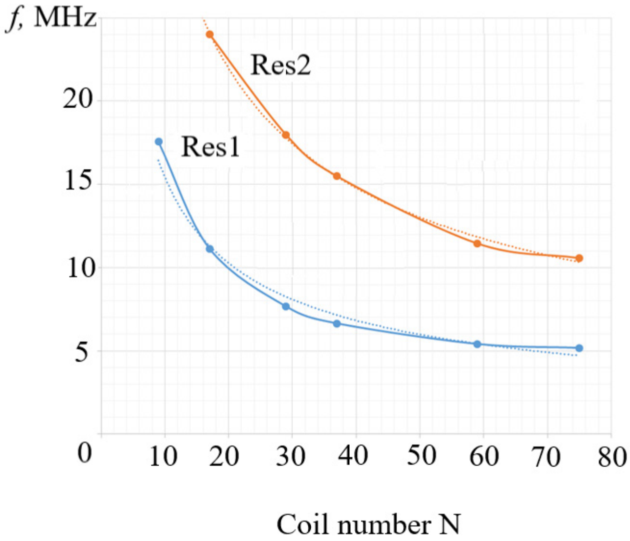

Fig. 9. Experimental (points) and approximating (lines) dependences of resonant frequency of the detector on the positions of the break points for the first (Res1) and second (Res2) resonances

Conclusion

In this paper, we propose to use a film inductor as a detector for incident high-speed microparticles. This configuration eliminates the need for complex multiplexer arrays commonly used in sensors of this type. The presented results of computer and laboratory simulation of this configuration indicate that the film inductor is suitable for detection of high-speed microparticles with sizes from 100 μm in CubeSat spacecraft.

Analyzing the results, we found that the location of the break point in the metal strip of the inductor coil can be determined by analyzing the resonance frequency shift on the frequency response curve. It is possible to reliably determine the location of the break if the number of the broken turn is greater than 5.

REFERENCES

1. **Ivanov N. N., Dobritsa D. B., Yaschenko B. Y.,** A new way of automated dust control of the external atmosphere of a spacecraft during thermal-vacuum testing, Sol. Syst. Res. 54 (7) (2020) 662–667.

2. **Mironov V. V., Tolkach M. A.,** Velocity and distribution on velocity of meteoroids and space debris particles in near-Earth space, Kosmicheskaya Tekhnika i Tekhnologii [Space Technology and Engineering]. (1 (36)) (2022) 125–143 (in Russian).

3. **Durin C., Mandeville J. C., Perrin J. M.,** Active detection of micrometeoroids and space debris SODAD-2 experiment on SAC-D satellite, Adv. Space Res. 69 (10) (2022) 3856–3863.

4. **Dmitryuk S. V.,** Space debris threat: Fundamental & practical aspects, Magazine VKS. (2(99)) (2019) 56–59 (in Russian).

5. **Shustov B. M.,** About fundamental research on space debris problem, In book: Proc. of All-Russian Conf. “Space Debris: Fundamental and Practical Aspects of the Threat”, Moscow, April 17–19 2019; Ser. “Mechanics, Management, Computer Science”, L. M. Zelenyi, B. M. Shustov (Eds.). Space research Institute of the RAS, Moscow (2019) 7–14 (in Russian).

6. **Ipatov A. V., Vedeshin L. A., Gerasyutin S. A.,** Monitoring kosmicheskogo musora i perspektivy osvoeniya okolozemnogo kosmicheskogo prostranstva [Space debris monitoring and prospects for the exploration of near-Earth space], Zemlya i Vselennaya [The Earth and Universe]. (2 (356)) (2024) 91–108 (in Russian).

7. **Adushkin V. V., Kozlov S. I., Aksenov O. Y., et al.,** The small orbital debris population and its impact on space activities and ecological safety, Acta Astronaut. 176 (Nov) (2020) 591–597.

8. **Rodmann J., Miller A., Traud M., et al.,** Micrometeoroid impact risk assessment for interplanetary missions, Proc. 8th Eur. Conf. on Space Debris (virtual), Darmstadt, Germany, 20—23 April 2021, T. Flohrer, S. Lemmens, F. Schmitz (Eds.), publ. by the ESA Space Debris Office; May (2021) 1 — 5.

9. **Agapov V. M., et al.,** Kosmicheskij musor.: V 2 kn. Red. Raykunov G. G., Kn.1. Metody nablyudeniya i modeli kosmicheskogo musora [Space debris: In 2 books. Raykunov G. G. (Ed.), Book 1. Methods of observation and models of space debris], FIzmatlit Publishing, Moscow, 2014 (in Russian).

10. **Novikov L. S.,** Osnovy ekologii okolozemnogo kosmicheskogo prostranstva [Fundamentals of ecology of the near-Earth space], Universitetskaya kniga [University Book Publishing], 2006 (in Russian).

11. **Kalaev M. P., Rodina A. V., Telegin A. M.,** Investigation of changes in the characteristics of solar panels under the influence of space factors, Instrum. Exp. Tech. 65 (6) (2022) 970—975.

12. **Kalaev M. P., Telegin A. M., Voronov K. E., et al.,** Investigation of optical glass characteristics under the influence of space factors, Computer Optics. 43 (5) (2019) 803—809 (in Russian).

13. **Wang, W., Xue, W., Wu S., et al.,** High-speed micro-particle motion monitoring based on continuous single-frame multi-exposure technology, Materials. 15 (11) (2022) 3871.

14. **Barilaro L., Falsetti C., Olivieri L., et al.,** A conceptual study to characterize properties of space debris from hypervelocity impacts through thin film heat flux gauges, Proc. 2021 IEEE International Workshop on Metrology for AeroSpace (MetroAeroSpace-2021). IEEE Inc. (2021) 430—435.

15. **Gola Y., Kim D., Namilae S.,** Piezoresistive nanocomposites for sensing MMOD impact damage in inflatable space structures, Compos. Commun. 21 (Oct) (2020) 100375.

16. **Rose R., Koets M., Chocron S., Grimm R.,** Application of intelligent spacecraft structures for impact detection, Proc. 2022 IEEE Aerospace Conference (AERO). 5 —12 March 2022. Big Sky, MT, USA (2022) 1—7.

17. **Gbaguidi A., Madiyar F., Kim D., Namilae S.,** Multifunctional inkjet printed sensors for MMOD impact detection, Smart Mater. Struct. 29 (8) (2020) 085052.

18. **Hofmann D. C., Bordeenithikasem P., Zhu Y., et al.,** Design, fabrication, and hypervelocity impact testing of screen-printed flexible micrometeoroid and orbital debris impact sensors for long-duration spacecraft health monitoring, Aerosp. Sci. Technol. 139 (Aug) (2023) 108372.

19. **Faure P., Masuyama Sh., Nakamotoa H., et al.,** Space dust impacts detector development for the evaluation of ejecta, Proc. Eng. 58 (2013) 594—600.

20. **Semkin N. D., Telegin A. M.,** Shock-compressed metal-insulator-metal structures under the action of fast dust particles, Tech. Phys. 56 (7) (2011) 986—991.

21. **Telegin A. M.,** Modeling the transmission coefficient of a micrometeoroid and space debris particle sensor, Eng. Phys. (4) (2024) 37—44 (in Russian).

22. **Bahl I. J.**, Lumped elements for RF and microwave circuits, Artech House Microwave Library, Boston, London, 2003.

23. **Boreyko D. A., D'yachenko T. S., Tyumentsev A. I.,** Issledovanie parametrov katushek induktivnosti, vypolnennyh po LTCC tekhnologii [Study of the parameters of inductance coils made using LTCC technology], Tekhnika radiosvyazi [Radio Commun. Technol.] (17) (2012) 73—83 (in Russian).

24. **Wheeler H. A.,** Simple inductance formulas for radio coils, Proc. Instit. Radio Eng. 16 (10) (1928) 1398—1400.

25. **Kalantarov P. L., Tseitlin L. A.,** Raschet induktivnostej: Spravochnaya kniga [Calculation of inductances: Reference book], 3rd edition, Enerroatomizdat Publishing. Leningrad, 1986 (in Russian).

26. **Benhadda Y., Derkaoui M., Mendaz K., et al.,** Design for integrated planar spiral inductor for MEMS, Period. Polytech. Electr. Eng. Comput. Sci. 67 (4) (2023) 425—437.

27. **Hussain I., Woo D.-K.,** Simplified mutual inductance calculation of planar spiral coil for wireless power applications, Sensors. 22 (4) (2022) 1537.

28. **Futai N., Futai N., Matsumoto K., Shimoyama I**., A flexible micromachined planar spiral inductor for use as an artificial tactile mechanoreceptor, Sens. Actuators A: Phys. 111 (2) (2004) 293—303.

29. **Berthoud L., Mandeville J.-C.,** Empirical impact equations and marginal perforation, Proc. First Eur. Conf. on Space Debris, Darmstadt, Germany. 5—7 April 1993. ESA SD-01 (1993) 459—464.

30. **Awang Z.,** Microwave systems design, Springer Science & Business Media, Berlin/Heidelberg, 2013.

31. **Benedek P., Silvester P.,** Equivalent capacitances for microstrip gaps and steps, IEEE Trans. Microw. Theory Tech. 20 (11) (1972)729 —733.

32. **Garg R., Bahl I. J.,** Microstrip discontinuities, Int. J. Electron. 45 (1) (1978) 81–87.

33. **Qiao Q., Dai Y., Chen Z.,** Signal integrity analysis on discontinuous microstrip line, J. Phys. Conf. Ser. (ICAES-2012). 418 (2013) 012087.

34. **Clayton R. P.**, Analysis of multiconductor transmission lines, Wiley& Sons, Inc., Hoboken, New Jersey, USA, 2008.

СПИСОК ЛИТЕРАТУРЫ

1. **Ivanov N. N., Dobritsa D. B., Yaschenko B. Y.** A new way of automated dust control of the external atmosphere of a spacecraft during thermal-vacuum testing // Solar System Research. 2020. Vol. 54. No. 7. Pp. 662–667.

2. **Миронов В. В., Толкач М. А.** Скорость и распределение скорости метеороидов и частиц космического мусора в околоземном космическом пространстве // Космическая техника и технологии. 2022. № 1 (36). С. 125–143.

3. **Durin C., Mandeville J. C., Perrin J. M.** Active detection of micrometeoroids and space debris SODAD-2 experiment on SAC-D satellite // Advances in Space Research. 2022. Vol. 69. No. 10. Pp. 3856–3863.

4. **Дмитрюк С. В.** Космический мусор: прикладные аспекты угрозы // Воздушно-космическая сфера. 99) 2 № .2019). С. 59–56.

5. **Шустов Б. М.** О фундаментальных исследованиях по проблеме космического мусора // Сборник трудов Всероссийской научной конференции «Космический мусор: фундаментальные и практические аспекты угрозы». 19–17 апреля 2019 г. Сер. «Механика, управление и информатика». Под ред. Л. М. Зеленого, Б. М. Шустова. М.: ИКИ РАН, 2019. С. 7 –14.

6. **Ипатов А. В., Ведешин Л. А., Герасютин С. А.** Мониторинг космического мусора и перспективы освоения околоземного космического пространства // Земля и Вселенная. 2024. № 2 (356). С. 91–108.

7. **Adushkin V. V., Kozlov S. I., Aksenov O. Y., Veniaminov S. S., Tyurenkova V. V.** The small orbital debris population and its impact on space activities and ecological safety // Acta Astronautica. 2020. Vol. 176. Novenber. Pp. 591–597.

8. **Rodmann J., Miller A., Traud M., Bunte K. D., Millinger M.** Micrometeoroid impact risk assessment for interplanetary missions // Proceedings of the. 8th European Conference on Space Debris (virtual), Darmstadt, Germany, 20–23 April 2021, T. Flohrer, S. Lemmens, F. Schmitz (Eds.), published by the ESA Space Debris Office; May 2021. Pp. 1 – 5.

9. **Агапов В. М. и др.** Космический мусор: В 2 кн. Под науч. ред. Г. Г. Райкунова. Кн.1. Методы наблюдения и модели космического мусора. М.: Физматлит, 2014. 244 с.

10. **Новиков Л. С.** Основы экологии околоземного космического пространства. М.: Университетская книга, 84 .2006 с.

11. **Калаев М. П., Родина А. В., Телегин А. М.** Исследование изменения характеристик солнечных батарей при воздействии факторов космического пространства // Приборы и техника эксперимента. 6 № .2022. С. 105–99.

12. **Калаев М. П., Телегин А. М., Воронов К. Е., Лисян Ц., Цзилун Ц.** Исследование характеристик оптических стекол при воздействии факторов космического пространства // Компьютерная оптика. 2019. Т. 43. № 5. С. 803 –809.

13. **Wang, W., Xue, W., Wu S., Mu Z., Yi J., Tang A. J.** High-speed micro-particle motion monitoring based on continuous single-frame multi-exposure technology // Materials. 2022. Vol. 15. No. 11. P. 3871.

14. **Barilaro L., Falsetti C., Olivieri L., Giacomuzzo C., Francesconi A., Beard P., Camilleri R.** A conceptual study to characterize properties of space debris from hypervelocity impacts through thin film heat flux gauges// Proceedings of the 2021 IEEE International Workshop on Metrology for AeroSpace, (MetroAeroSpace- 2021). IEEE Inc. 2021. Pp. 430–435.

15. **Gola Y., Kim D., Namilae S.** Piezoresistive nanocomposites for sensing MMOD impact damage in inflatable space structures // Composites Communications. 2020. Vol. 21. October. P. 100375.

16. **Rose R., Koets M., Chocron S., Grimm R.** Application of intelligent spacecraft structures for impact detection // Proceedings of the 2022 IEEE Aerospace Conference (AERO). 5 –12 March 2022. Big Sky, MT, USA. 2022. Pp. 1–7.

17. **Gbaguidi A., Madiyar F., Kim D., Namilae S.** Multifunctional inkjet printed sensors for MMOD impact detection // Smart Materials and Structures. 2020. Vol. 29. No. 8. P. 085052.

18. **Hofmann D. C., Bordeenithikasem P., Zhu Y., Liu Y., Conrad N. J., Davis B. A., Christiansen E. L., Shakouri A., Mohammadi S.** Design, fabrication, and hypervelocity impact testing of screen-printed flexible micrometeoroid and orbital debris impact sensors for long-duration spacecraft health monitoring // Aerospace Science and Technology. 2023. Vol. 139. August. P. 108372.

19. **Faure P., Masuyama Sh., Nakamotoa H., Akahoshi Y., Yukihito Kitazawa Y., Koura T.** Space dust impacts detector development for the evaluation of ejecta // Procedia Engineering. 2013. Vol. 58. Pp. 594–600.

20. **Семкин Н. Д., Телегин А. М.** Ударно-сжатые структуры металл-диэлектрик-металл в условиях воздействия высокоскоростных пылевых частиц // Журнал технической физики. 2011. Т. 7 № .81. С. 93–88.

21. **Телегин А. М.** Моделирование коэффициента передачи датчика микрометеороидов и частиц космического мусора // Инженерная физика. 2024. № 4. С. 37–44.

22. **Bahl I. J.** Lumped elements for RF and microwave circuits. Boston, · London: Artech House Microwave Library, 2003. 488 p.

23. **Борейко Д. А., Дьяченко Т. С., Тюменцев А. И.** Исследование параметров катушек индуктивности, выполненных по LTCC технологии // Техника радиосвязи. 2012. № 17. С. 73–83.

24. **Wheeler H. A.** Simple inductance formulas for radio coils // Proceedings of the Institute of Radio Engineers. 1928. Vol. 16. No. 10. Pp. 1398–1400.

25. **Калантаров П. Л., Цейтлин Л. А.** Расчет индуктивностей: Справочная книга. 3-е изд., перераб. и доп. Ленинград: Энергоатомиздат, 1986. 488 с.

26. **Benhadda Y., Derkaoui M., Mendaz K., Kharbouch H., Spiter P.** Design for integrated planar spiral inductor for MEMS // Periodica Polytechnica Electrical Engineering and Computer Science. 2023. Vol. 67. No. 4. Pp. 425–437.

27. **Hussain I., Woo D.-K.** Simplified mutual inductance calculation of planar spiral coil for wireless power applications // Sensors. 2022. Vol. 22. No. 4. P. 1537.

28. **Futai N., Futai N., Matsumoto K., Shimoyama I**. A flexible micromachined planar spiral inductor for use as an artificial tactile mechanoreceptor // Sensors and Actuators A: Physical. 2004. Vol. 111. No. 2. Pp. 293–303.

29. **Berthoud L., Mandeville J.-C.** Empirical impact equations and marginal perforation // Proceedings of the First European Conference on Space Debris, Darmstadt, Germany. 5–7 April 1993. ESA SD-01. Pp. 459–464.

30. **Awang Z.** Microwave systems design. Berlin/Heidelberg: Springer Science & Business Media, 2013. 313 c.

31. **Benedek P., Silvester P.** Equivalent capacitances for microstrip gaps and steps // IEEE Transactions on Microwave Theory and Techniques. 1972. Vol. 20. No. 11. Pp.729 –733.

32. **Garg R., Bahl I. J.** Microstrip discontinuities // International Journal of Electronics. 1978. Vol. 45. No. 1. Pp. 81–87.

33. **Qiao Q., Dai Y., Chen Z.** Signal integrity analysis on discontinuous microstrip line // Journal of Physics: Conference Series. 7th International Conference on Applied Electrostatics (ICAES-2012). 2013. Vol. 418. P. 012087.

34. **Clayton R. P.** Analysis of multiconductor transmission lines. Hoboken, New Jersey, USA: Wiley& Sons, Inc., 2008. 821 p.

THE AUTHORS

TELEGIN Aleksey M.
Samara National Research University
34 Moscow HWy, Samara, 443086, Russia
talex85@mail.ru
ORCID: 0000-0002-1750-1536

KALAEV Mikhail P.
Samara National Research University
34 Moscow HWy, Samara, 443086, Russia
sgau5@yandex.ru
ORCID: 0009-0003-2601-4144

СВЕДЕНИЯ ОБ АВТОРАХ

ТЕЛЕГИН Алексей Михайлович – *кандидат физико-математических наук, доцент кафедры радиоэлектронных систем Самарского национального исследовательского университета имени академика С. П. Королёва.*
443086, Россия, г. Самара, Московское шоссе, 34
talex85@mail.ru
ORCID: 0000-0002-1750-1536

КАЛАЕВ Михаил Павлович – *кандидат технических наук, доцент кафедры радиоэлектронных систем Самарского национального исследовательского университета имени академика С. П. Королёва.*
443086, Россия, г. Самара, Московское шоссе, 34
sgau5@yandex.ru
ORCID: 0009-0003-2601-4144

Received 20.01.2025. Approved after reviewing 10.03.2025. Accepted 10.03.2025.
Статья поступила в редакцию 20.01.2025. Одобрена после рецензирования 10.03.2025. Принята 10.03.2025.